PAIN MEDICINE
Volume 6 • Number 6 • 2005

SPECIAL ARTICLE

Electric and Thermal Field Effects in Tissue Around Radiofrequency Electrodes

Eric R. Cosman, Jr., MEng, PhD,* and Eric R. Cosman, Sr., PhD, Prof.**

Departments of *Electrical Engineering and Computer Science and **Physics, Massachusetts Institute of Technology, Cambridge, Massachusetts, USA

ABSTRACT

Objective. A study is carried out of the spatial distribution and time dependence of electric and thermal fields in the tissue around a radiofrequency (RF) electrode used in pain therapy. Finite-element calculation of the fields is performed, and results are compared with ex vivo tissue data. Field predictions are made for continuous and for pulsed RF applications.

Design. A special RF cannula electrode is constructed with both macro and micro thermocouple sensors to measure both average and rapid, transitory temperature effects. Temperatures and impedances are recorded in liver and egg-white models using signal outputs from a commercially available RF lesion generator. These data are compared with the results of finite-element calculations using electric field equations and the bio-heat equation.

Results. Average and pulsatory temperatures at the RF electrode are measured. Rapid temperature spikes during pulsed RF bursts are observed. These data compared well with theoretical calculations using known electrical and thermal tissue parameters.

Conclusion. Continuous RF lesioning causes heat destruction of neurons. Pulsed RF lesioning (PRFL) produces heat bursts with temperatures in the range associated with destructive heat lesions. PRFL also produces very high electric fields that may be capable of disrupting neuronal membranes and function. Finite-element calculations agree substantially with the measured data, giving confidence to their predictions of fields around the RF electrode.

Key Words. Radiofrequency Lesion; Pulsed Radiofrequency; Temperature Distributions; Electric Fields; Finite-Element Calculations

Introduction

The application of radiofrequency (RF) electric signals to neural tissue by means of an RF lesion generator and RF electrodes inserted into the tissue is a well-established technique. The technique is employed to treat pain, movement, and mood disorders. The usual objective is to deposit enough RF heating power into the tissue to raise the temperature of the targeted tissue above 45–50°C. This is referred to as the "lethal temperature range" as cell structures exposed to these temperatures for 20 seconds or more are known to be destroyed by the heat.

The earliest RF lesion generators and electrodes were built by B. J. Cosman, S. Aranow, and O. A. Wyss in the early 1950s. Their devices all used continuous-wave RF power sources in the 0.1–1 MHz frequency range to produce the RF heat lesions, and the commercial RF generators of

Reprint requests to: Eric R. Cosman, Sr., Prof., 872 Concord Avenue, Belmont, MA 02478, USA. Tel: 781-272-6561; Fax: 781-272-6563; E-mail: ecosman@cosmancompany.com.

 1526-2375/05/$15.00/405 405–424

today use that same frequency range. This method will be referred to here as CRFL, standing for "continuous RF lesioning." The practical aspects of the CRFL methods are now well established [1,2]. Its underlying physical principles and the expected size and shape of the RF heat lesions for different electrode geometries and temperatures are understood [3].

A more recent RF method for the treatment of pain applies short pulses of RF signals from an RF generator to the neural tissue through the RF electrode [4]. This is referred to here as PRFL, standing for "pulsed RF lesioning." Commercially available RF lesion generators provide PRFL signals with pulse durations ranging from 10 to 30 ms, and pulse repetition rates ranging from 1 to 8 Hz (pulses per second). The underlying RF frequency within each pulse is typically about 500 KHz, which is the same as for CRFL.

Because the RF pulse duration is only a small percentage of the time between pulses in PRFL, the average tissue temperature rise for the same RF voltage on the same electrode is less for PRFL than for CRFL. For the same reason, higher RF voltages can be applied to the electrode in PRFL than are commonly used in CRFL without raising the average tissue temperature near the electrode into the "lethal temperature range," that is, at or above 45–50°C. This has been the approach used by most clinicians performing PRFL. It has led to PRFL being loosely described by some as a "nonthermal lesion," or as a "nondestructive" process. The implied assumption is that heat is not causing any clinical effect or any destructive effect in PRFL, but rather that there are some other nondestructive agents that account for all effects seen from PRFL. The suggestion has been made that the other physical agents are the high electric fields and currents present in PRFL [4].

An objective of the present study is to put the understanding of the processes of CRFL and PRFL on a more quantitative footing based on the underlying physical mechanisms that are common to both. It is our view that during the RF pulses in PRFL, there should be temperature bursts in the tissue. We find them to exist and find their temperatures to extend into the "lethal temperature range" in some cases. This result draws into question the extent to which PRFL may be considered a totally "nonthermal lesion" or totally "nondestructive." To understand what effects high PRFL electric fields and currents may have on neurons, the magnitude of these quantities should be determined. We do this in the present study by theoretical predictions using a physical model which we demonstrate to correctly describe measurable aspects of RF lesioning, such as tip temperatures, time dependencies, and impedances. We also calculate the magnitude of transmembrane potentials induced by the electric field. We discuss the possibility that these potentials may be capable of producing electroporation. We also discuss the possibility that they may produce ion channel rectification leading to low-level stimulation and thus long-term depression of nociception.

Methods

The Calculation of the Electric and Thermal Fields

The calculation of the electric field vector **E** around an RF electrode placed in a conductive, dielectric medium such as tissue is governed by Maxwell's equations. The E-field gives rise to electric forces on mobile ions in the tissue electrolytes which in turn produce the current density vector field **j** within the tissue given by:

$$\mathbf{j} = \sigma \mathbf{E}$$

where σ is the specific electrical conductivity of the tissue. At low RF frequencies of 500 KHz, the average power deposition density from ohmic friction is:

$$P = \frac{0.5|\mathbf{j}|^2}{\sigma} = 0.5\sigma E^2$$

where E is the amplitude of **E**, which is assumed to be oscillating with the RF frequency. The distribution of temperature T in the tissue can be calculated using the bio-heat equation:

$$\rho C_p \frac{\partial T}{\partial t} = 0.5\sigma E^2 + \nabla \cdot (k \nabla T) + W_b C_b (T_b - T)$$

The left-hand side of the equation is the rate of change of the heat energy density, where C_p is the heat capacity per unit mass, and ρ is the mass density. The first term on the right is the power deposition density. The second term on the right side is the conductive heat loss per unit volume, where ∇ is the gradient operator, and k is the thermal conductivity. The third term on the right is the heat loss from blood convection, where W_b is the mass flow density for blood, C_b is the specific heat of blood, and T_b is the normal blood temperature of 37°C.

The electric field **E** is calculated first and then put into the bio-heat equation to calculate T. The E-equation that governs **E** at RF frequency f is:

$$\nabla \cdot (\sigma + i\omega\varepsilon\varepsilon_0)\mathbf{E} = 0$$

where $i = \sqrt{-1}$, $\omega = 2\pi f$ is the RF angular frequency, ε is the relative permittivity of the tissue, and $\varepsilon_0 = 8.85 \times 10^{-12}$ Farads/m is the permittivity of free space. The E-field is oscillating at RF angular frequency ω, and in complex notation it is written:

$$\mathbf{E} = Ee^{i\omega t}\mathbf{u}$$

where E is the amplitude of the E-field at each point in space, and $\mathbf{u}$ is the unit vector in the direction of $\mathbf{E}$. The E-equation combines Gauss' Law and charge conservation in complex number notation. It does not account for currents induced by time-varying magnetic fields, which are negligible at low RF frequencies.

The E-equation is simplified by introducing the electric potential Φ from which $\mathbf{E}$ can be derived by:

$$\mathbf{E} = -\nabla\Phi$$

The E-equation then becomes the Φ-equation:

$$\nabla \cdot [(\sigma + i\omega\varepsilon\varepsilon_0)\nabla\Phi] = 0$$

where Φ is a complex number.

The Φ-equation can be solved for a given model of an RF electrode and its surrounding medium by finite-element methods with a computer program. The values of σ, ω, and ε are input parameters. The geometry of the electrode model imposes input boundary conditions. Electrical boundary conditions include the amplitude of Φ values being constant on the electrode tip surface (and equal to the RF voltage from the RF generator on the electrode), the Φ values being constant (zero) at the reference surfaces far from the electrode, and the $\mathbf{E}$ vector being parallel to insulative surfaces (viz. the insulated shaft of the electrode).

The bio-heat equation can be solved for T also with finite-element methods, using $\mathbf{E}$ and the values of C_p, ρ, σ, k, W_b, C_b, and T_b as input parameters.

Finite-element methods are well known [5]. Existing computer programs are available to solve the Φ, $\mathbf{E}$, and bio-heat equations. Calculations here are performed using the program ETherm [6]. Physical and geometric parameters for these calculations are specified below.

The RF Electrode

To assess the validity of the RF field and temperature calculations, experimental measurements have been made of temperature, impedance, and other electrical parameters associated with an RF electrode placed into beef liver and egg-white during application of CRFL and PRFL signals. The electrode system chosen was an SMK-C10-5 cannula of COTOP International (The Netherlands), which is commonly used for medial branch and dorsal root ganglion (DRG) RF treatments. It is a 22-gauge stainless steel cannula with 0.7-mm exposed tip diameter, 5-mm exposed tip length, and otherwise an insulated shaft. The tip has about an 18° bevel with sharpened distal point. In normal use, the SMK-TC thermocouple electrode of Radionics, Inc. (Burlington, MA), which comprises a 0.36-mm diameter stainless steel shaft with indwelling thermocouple, is inserted into the SMK cannula to measure tip temperature during RF lesioning.

In the present experiments, a second micro-TC thermocouple has been added as shown in Figure 1. Its purpose is to detect very fast tissue temperature changes at the sharpened point of the cannula bevel. The micro-TC sensor is fused to the sharpened point of the SMK cannula. The effective volume of the micro-TC sensor, which is the combined volume of thermocouple material and cannula point volume to which it is attached, is $0.05 \times 0.05 \times 0.04$ mm^3 or 10^{-4} mm^3. The micro-TC is in direct contact with the heated tissue. In contrast, the macro SMK-TC sensor is typically inside the bevel tip margin (and thus not in direct contact with tissue), and it is surrounded by the 22-gauge SMK-C10-5 cannula tubing. Its effective thermal sensing volume is approximately 0.5 mm^3, which is about 5,000 times larger than the micro-TC volume. Thus, it is expected that the SMK-TC sensor will have at least a 1,000 times slower

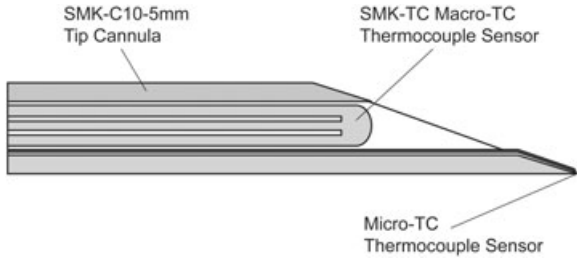

Figure 1 A diagram in section view through the RF electrode used in the liver and egg-white measurements of *Z* and *T*. The SMK-TC(10) cannula with 5-mm exposed tip is commonly used for RF pain procedures. The SMK-TC is also standard and is a macro-TC thermocouple to detect average temperatures. The micro-TC is added to detect rapid *T*-spikes during PRFL. RF = radiofrequency; PRFL = pulsed RF lesioning.

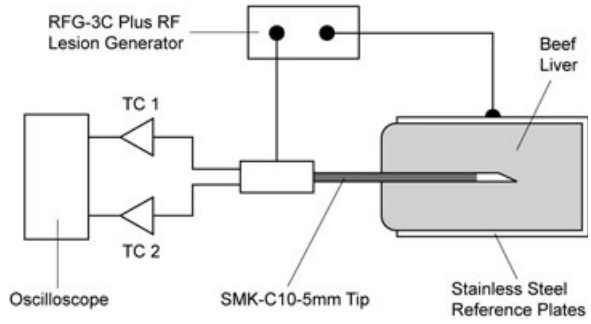

Figure 2 A schematic diagram of the experimental setup for measuring the average temperature from the SMK-TC macro-TC thermocouple and the rapid heat spikes from the micro-TC thermocouple during RF application with the SMK-C(10)-5 mm electrode in ex vivo liver. RF = radiofrequency.

thermal response time than the micro-TC sensor and will be incapable of detecting millisecond temperature changes anticipated in PRFL.

The Electrical and Thermal Measurements

To simulate the electrical environment encountered in living neural tissue, measurements were made in fresh beef liver and in egg-white. The liver has a cellular matrix with known σ and ε values in a similar range to soft tissue near and in the spinal nerve and medial branch. The egg is more similar to bodily electrolytes such as CSF or intracellular fluids.

Figure 2 shows the experiment setup used for the liver measurements. The SMK-C10-5 cannula, modified with the micro-TC sensor, is inserted into a slab of liver approximately 5–6 cm thick and 10×10 cm^2 in area. RF output is supplied to the cannula by an RFG-3C Plus RF lesion generator (Radionics, Inc.). The usual C112-TC cable connection is made to the SMK cannula, and reference connections are made to stainless steel plates on the top, bottom, and sides of the liver slab. Two rapid thermocouple readout circuits, TC1 and TC2, measure the temperatures for the micro-TC and the macro-TC SMK-TC thermocouples, respectively. The TC1 and TC2 readings are displayed on a Tektronix oscilloscope. The TC1 and TC2 recordings and the values of RF voltage V, RF current I, and impedance Z as displayed by the RFG-3C Plus lesion generator were recorded for each measurement session.

The setup for the egg-white measurements was similar to that in Figure 2, except that a Nikon microscope with ×40 power with a SONY CCD color video camera display and a SONY color video frame capture printer were used to visualize and record evidence of temperature features.

Because the comparison of the calculated versus the measured heat spikes in PRFL depends sensitively on impedance, an independent measurement of Z was made using the setup in Figure 3. A nonreactive reference resister R_{ref} was put in series with the electrode and tissue load impedance Z, and the amplitudes of voltages V_1 and V_2 were measured. The impedance is then:

$$Z = R_{ref} \frac{V_2}{V_1}$$

The phase angle θ between V_1 and V_2 can be non-negligible for cellular tissues at $f = 500$ KHz, and θ was also measured here. The resistive component R of the tissue (load) impedance Z, which is relevant to calculate heat spike amplitude in PRFL, can then be determined by:

$$R = Z \cos \theta$$

A consistency check of the field calculations is that the measured value of Z should agree with the value calculated assuming tissue conductivity σ and permittivity ε. Further, the calculated and measured heat spikes in PRFL should agree and be proportional to $V(\text{peak})^2/2R$, where $V(\text{peak})$ is the peak RF voltage on the electrode.

Finite-Element Model Parameters

The SMK-C10-5 electrode model used in the calculations is shown in Figure 4. The stainless steel

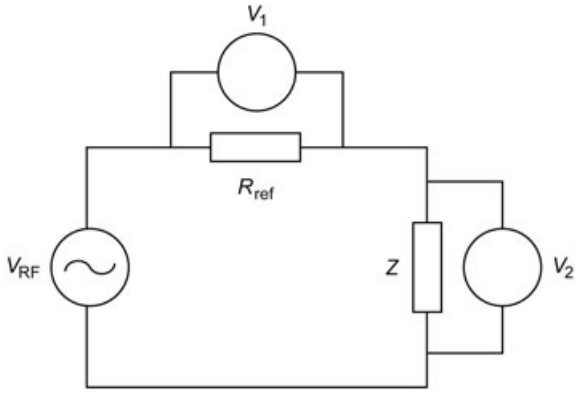

Figure 3 A schematic diagram of the system for measuring the complex impedance of a sample load Z, which here is liver or egg-white. R_{ref} is the reference, resistance, the circles near V_1 and V_2 represent their readings by an oscilloscope, and V_{RF} is the RF voltage source. RF = radiofrequency.

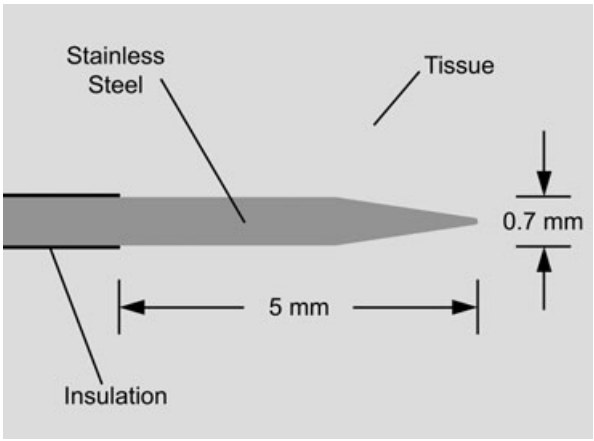

Figure 4 A schematic diagram of the electrode and tissue model used in the finite-element calculations. A reference surface with fixed potential of zero is located on a closed rectangular perimeter well outside the field of view.

shaft has an outer diameter of 0.7 mm like the SMK cannula. The calculation is for rotational symmetry, so the SMK cannula bevel is simulated by a conical point with 18° included angle. A finite point radius of 0.05 mm is assumed to avoid an infinite singularity, although this radius is arbitrary and does not strongly affect the calculated results. The exposed RF tip is 5 mm long, and the insulation is 0.05 mm thick. The steel shaft is modeled as a solid because the SMK cannula is used with the SMK-TC steel tubing within it, approximating a solid metal interior space. The metal is an equipotential, and the value of Φ is fixed throughout the metal at the RF voltage output V of the RF generator.

The electrical and thermal parameters for the model materials in the liver and egg-white calculations are shown in Table 1. The units are shown in the table, and throughout this article if a parameter is given without units, it is assumed to have units as shown in Table 1.

Results

Impedance Measurements

Measurement of impedance magnitude Z, phase angle θ, and resistance R of the electrode in liver and egg-white provide a global check on the validity of model calculations and are necessary to compute E- and T-fields. The RFG-3C Plus generator displays Z at 50 KHz (referred to here as $Z_{3C}(50)$). It also displays V(rms) and I(rms) (rms means root-mean-square value) at 512 KHz for CRFL, and because $Z = V(\text{rms})/I(\text{rms})$, this provides a value of Z at 512 KHz (referred to here as $Z_{3C}(V/I)$). Some variability in the measured values is seen because of the position of the electrode in the liver and egg-white. At $T = 20°C$, $Z_{3C}(50)$ typically ranged from 450 to 650 Ω in liver and 115 to 120 Ω in egg-white. Typically, $Z_{3C}(50)$ is 1.1–1.3 times $Z_{3C}(V/I)$, both for liver and egg-white. This difference is accounted for in part because Z at 512 KHz should be higher than Z at 50 KHz; however, some inaccuracies exist in the RFG-3C Plus measurement algorithm for $Z_{3C}(50)$ and $Z_{3C}(V/I)$, and they contribute to the difference.

The more precise and reliable method of measuring impedance described in the Methods section also determines Z at 512 KHz (referred to here as $Z_m(512)$). For liver, some variation in $Z_m(512)$ values are also seen depending on the electrode position in the liver and the ambient liver temperature. For the SMK-C(10) electrode with 5 mm tip at $T = 20°C$, $Z_m(512)$ was measured to be 220–350 Ω. On the average, $Z_{3C}(50)$ is 1.6–1.9 times $Z_m(512)$ for liver.

For egg-white at $T = 20°C$, $Z_{3C}(50)$ is 115–120 Ω, $Z_{3C}(V/I)$ is 98–105 Ω, and $Z_m(512)$ is about 110 Ω. Thus, $Z_{3C}(50)$ is about 1.15–1.2 times $Z_{3C}(V/I)$, and $Z_{3C}(50)$ is about 1.1 times $Z_m(512)$.

For liver, the phase angle θ between the pure resistance R and the complex vector $\mathbf{Z}$ is measured to be about 30°–40°, so R is 0.76–0.86 times Z; that is, in this data, R is about 176–280 Ω for liver. The positive θ phase angle in liver is a direct evidence of the liver cell membrane and results from the membrane's capacitive reactance. The measured θ value of 30°–40° is consistent with the value of 27° measured by Ludt and Herrmann [7].

Table 1 Input parameters to the finite-element calculations

Material	Quantity	Value	(units)
Liver	C_p, heat capacity	3,400	J/kg °C
	ρ, density	1,000	kg/m^3
	σ, electrical conductivity	0.29*	S/m
	ε, relative permittivity	2,000	—
	k, thermal conductivity	1.2	W/m °C
	W_b, blood perfusion	10	kg/m^3 s
Insulation	C_p, heat capacity	3,400	J/kg °C
	ρ, density	800	kg/m^3
	σ, electrical conductivity	0	S/m
	ε, relative permittivity	2.7	—
	k, thermal conductivity	0.01	W/m °C
Stainless steel	C_p, heat capacity	500	J/kg °C
	ρ, density	7,900	kg/m^3
	k, thermal conductivity	15	W/m °C

* This value was used for all PRFL calculations. For CRFL calculations shown in Figure 8, an effective $\sigma(\text{eff}) = 0.38$, 0.44, and 0.47 was used to calculate the average temperature increase $\Delta T(\text{avg})$ after 120 seconds for the cases $V(\text{rms}) = 7$, 13, and 16 V, respectively.
CRFL = continuous radiofrequency lesioning; PRFL = pulsed radiofrequency lesioning.

For neural tissue, θ will differ from that of liver because of the different cell geometry.

For egg-white, the measured phase angle θ is zero. This is because there are no cells (and therefore no cell membranes) in egg-white, and the impedance is purely resistive.

For liver, the calculated value of R using $\sigma = 0.29$ and $\varepsilon = 2{,}000$ is $R = 276\ \Omega$. This is in good agreement with the measured values of R, which was in the range 176–280 Ω. The assumed value of $\sigma = 0.29$ is also in good agreement with the published value of $\sigma = 0.3$ at 20°C reported by Foster and Schwan [8] at 500 KHz.

It is well known that R, σ, k, and C_p are temperature-dependent. This is obvious from clinical experience where to hold a fixed T at the electrode in a CRFL or a PRFL application, the RF voltage V must be steadily decreased. This is to stabilize the power $P = 0.5V(\text{peak})^2/R$. Evidently, R is decreasing with increasing T and therefore V^2 must be decreased to maintain P and T approximately constant.

Cosman et al. [9] have measured the Z versus T curves for RF electrodes in saline, ex vivo beef, egg-white, and in vivo brain. The value of Z at a given electrode temperature is an integration of tissue impedances at different temperature zones around the electrode. Thus, an exact relationship of Z to σ is not simple. The full time- and space-dependent variation of input parameters is not done in the present calculation. Instead, an effective value of σ for different equilibrium temperatures T, designated $\sigma(\text{eff})$, is assumed to be constant in the bio-heat equation to compute variations in T as a function of distance and time. For example, in calculating CRFL asymptotic lesions and for asymptotic temperature T_A after $t = 120$ seconds, a $\sigma(\text{eff})$ is assumed constant during the lesion time, and $\sigma(\text{eff})$ is increased with increasing T_A. $\sigma(\text{eff})$ is assumed to have an approximate T_A-dependence proportional to $1/Z(T_A)$ where $Z(T_A)$ is determined in [9]. The result for liver is:

$$\sigma(\text{eff}) \cong 0.29 + 0.0051(T_A - 20)$$

where the constant 0.29 is fixed by $\sigma(\text{eff}) = 0.29$ at 20°C as determined here, and units of $\sigma(\text{eff})$ being S/m. The values of k and C_p are assumed to be constant in this study. In the PRFL calculations, a fixed $\sigma(\text{eff}) = 0.29$ is used.

The Average Electric and Thermal Fields in the Liver

Figure 5 shows the electric field calculated from the above E-equation. The distribution of lines indicates the direction of the **E** vector, and the color tones indicate the magnitude E corresponding to the calibration in V/m units. The peak RF voltage $V(\text{peak}) = 45$ V is maintained on the electrode. The **E** vectors stream outward essentially radially and perpendicular to the electrode axis near the cylindrical mid-section of the tip, and their intensity E falls off with the $1/r$ dependence (r being the radial distance from the axis) near the cylinder. E tends to be intense at sharp points, sharp edges, end points, and boundaries insulation. This is evident in Figure 5 where E is stronger at the two ends of the tip. This is in part because like-charges aggregate on the metal surface during each RF voltage swing. Because like-charges are mutually repulsive, they concentrate at locations of farthest separation, that is, at the ends of the tip. Furthermore, at the pointed tip the curvature of the metal boundary is much higher, resulting in larger potential gradients $\nabla\Phi$ and thus the most intense electric fields. Note that near the insulation edge, **E** bunches up and curves over longitudinally so that **E** and **j** are parallel to the insulated shaft in order that no current **j** can pass normally to and thus into the insulation. The pattern of the **E** vectors in a homogeneous medium will not change significantly with V, σ, ε, or for CRFL or PRFL modes. However, the intensities E of the **E** vectors scale are essentially in direct proportion to the RF voltage V.

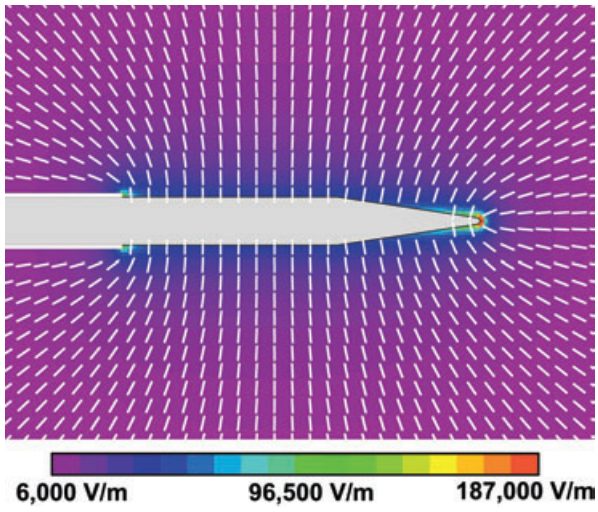

Figure 5 The directional pattern and intensity distribution of the E-field predicted by model calculation. The assumed RF voltage on the electrode is 45 V. The color intensity scale is shown at the bottom in units of V/m. RF = radiofrequency.

Figure 6 shows the average thermal field in liver calculated with the bio-heat equation. The color indicates temperature, and the color scale is shown on the left. To compare CRFL and PRFL, typical RF voltages of V(rms) = 13 V for CRFL and V(peak) = 70 V for PRFL are used. An ambient T = 37°C is used. The temperature T-fields for CRFL are shown in the upper half of each figure, and the T-fields for PRFL are shown in the lower half.

The calculated increase in temperature T for CRFL at t = 10, 30, and 60 seconds after output V is turned are shown in Figure 6(A), (B), and (C), respectively. In Figure 6(D), a line is shown which corresponds to the calculated 50°C isotherm. For CRFL with V(rms) = 13 V, E = 19,100 V/m on the mid-point surface of the electrode, and E = 2,500 V/m at a lateral point on the 50°C isotherm. Inside the SMK cannula T = 64°C at 60 seconds as would be measured by the SMK-TC probe. The 50°C isotherm is approximately the border of the heat lesion volume, because inside that isotherm, T > 50°C and all tissues are destroyed, although if T = 45°C is considered to be the lethal threshold, the heat lesion border would extend out further.

Figure 6 agrees with existing knowledge about CRFL lesion shapes [3]. The isotherms are prolate-ellipsoids of revolution for which the major axis (electrode axis) and minor axis (lateral radius) depend on electrode dimensions and RF voltage. The 50°C isotherm extends forward about 1 mm beyond the tip point and about the same distance backward from the insulation margin. Laterally, the 50°C isotherm extends about 2 mm from the axis. Thus, the lesion size to the 50°C isotherm is 4 mm wide and 7 mm long. Defining the lesion volume at the 45°C isotherm would increase those dimensions by about 1 mm. At higher voltage V, the 50°C isotherm approaches sphericity, provided T at the electrode does not exceed 100°C.

The size of the 50°C isotherm, that is, the RF lesion volume, grows with time for RF voltage V. It approaches its equilibrium (or asymptotic) size in about 60–120 seconds for electrodes of the size of the SMK electrode. Leaving the V on for longer than that will not significantly increase the lesion size. The width of the 45–50°C isotherm calcu-

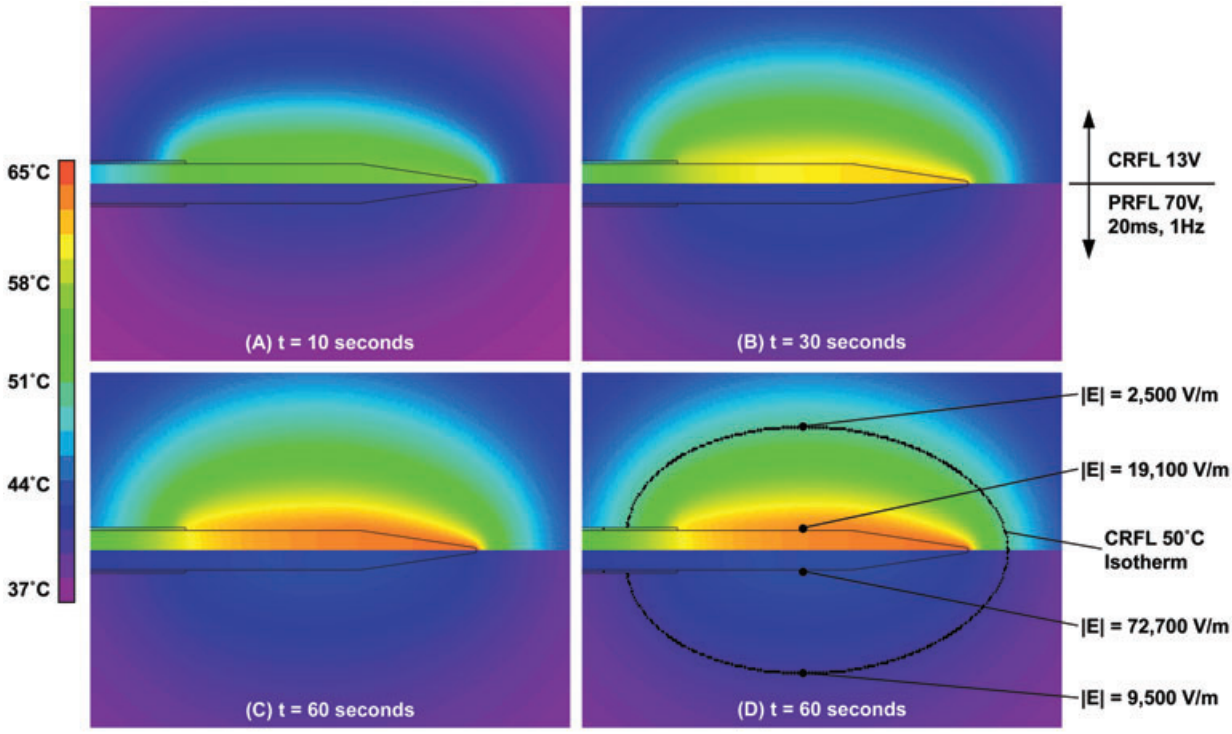

Figure 6 The calculated average temperature distributions are shown at t = 10, 30, and 60 seconds after applying RF voltage for the CRFL case (upper half of each figure) and for the PRFL case (lower half of each figure), Figure 6(A), (B), and (C), respectively. For CRFL the V(rms) = 13 V, and for PRFL the V(peak) = 70 V. The 50°C isotherm line is shown in Figure 6(D) and E values are indicated at selected positions. RF = radiofrequency; CRFL = continuous RF lesioning; PRFL = pulsed RF lesioning.

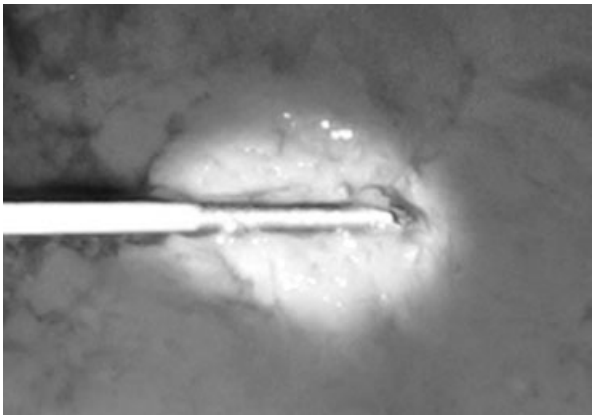

Figure 7 A photograph of the color-change in liver following a CRFL exposure using an SMK-TC(10)-5 mm electrode that is seen in the liver. The color change border represents an isotherm line. CRFL = continuous radiofrequency lesioning.

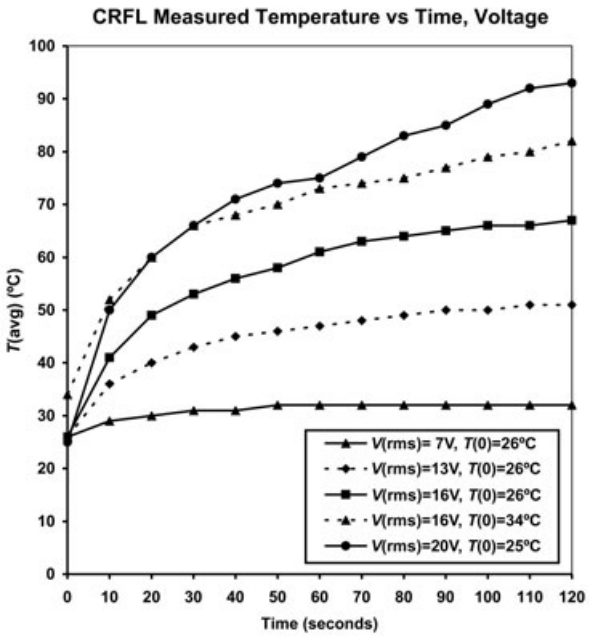

Figure 8 Average temperature versus time measurements for various fixed CRFL V(rms) settings using the SMK-TC(10)-5 mm electrode in liver. CRFL = continuous radiofrequency lesioning.

lated here is about 50% larger than data shown from postmortem studies in the brain [2]. This could easily be accounted for by the smaller σ for liver versus brain, by tissue shrinkage years after lesioning, and by an additional decrease of size of 15% estimated from in vivo blood perfusion (see Figure 16 below).

Figure 6 also shows the average temperature in liver for the PRFL case (the lower half of each figure). For peak RF voltage V(peak) = 70 V, pulse duration $D = 20$ ms and pulse repetition rate $N = 1$ Hz, there is only about a 5°C increase in the average T near the electrode after $t = 60$ seconds. This is consistent with PRFL average temperature increases in often-used clinical practice. Of significance are the very much stronger E-fields in the PRFL versus CRFL case. At the same medial and lateral distances, as noted for the CRFL case, the electric fields for PRFL are $E = 72{,}700$ V/m at the mid-tip surface and $E = 9{,}500$ V/m at a lateral distance of about 2.2 mm. These are over 3.8 times the value for the CRFL case discussed above.

Figure 7 is a photograph of the CRFL heat lesion shape in ex vivo liver using a SMK-C10 cannula with 5 mm tip, V(rms) = 20 V, and $t = 120$ seconds. The ambient liver temperature of 21°C and the temperature at which liver changes color are unrelated to the 45–50°C lesion point in neural tissue. However, Figure 7 shows that the shape of this particular color-change isotherm in liver agrees qualitatively with the predictions in Figure 6.

Figure 8 shows the average temperature T(avg) measured by the SMK-TC sensor in the electrode tip versus time for several values of V(rms). The voltage is increased manually and rapidly to V(rms) and held constant for 120 seconds. Two curves for V(rms) = 16 V are shown in different ambient liver temperatures of $T = 26$°C and $T = 34$°C, corresponding to starting impedances of $Z = 500\ \Omega$ and $Z = 448\ \Omega$, respectively. The curves are not simply parallel and offset by 8°C, but rather diverge by 15°C at $t = 120$ seconds. This indicates a nonlinear T-dependence of parameters such as σ and k. The measured change ΔT(avg) in T(avg) from its starting value after 120 seconds is given in Table 2, along with the calculated values of ΔT(avg) assuming the listed σ(eff) values. The agreement for ΔT(avg) is good, and σ(eff) is close to the guideline formula given above.

Table 2 Calculated and measured temperature rises for CRFL

RMS Voltage (V)	σ(eff) Electrical Conductivity (S)	Calculated ΔT(avg) at 120 seconds (°C)	Measured ΔT(avg) at 120 seconds (°C)
7	0.38	6.8	7
13	0.44	27.7	26
16	0.47	44.8	41, 48

CRFL = continuous radiofrequency lesioning

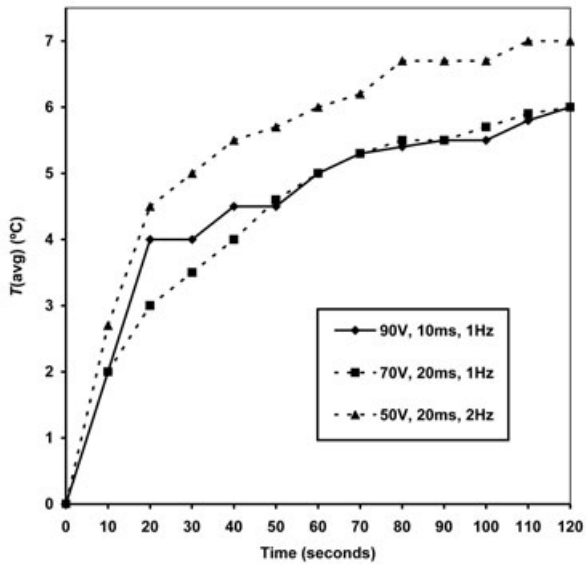

Figure 9 Average temperature versus time measurements for fixed PRFL *V*(peak) settings using the SMK-TC(10)-5 mm electrode in liver. PRFL = pulsed radiofrequency lesioning.

Figure 9 shows the average tip temperature change ΔT(avg) versus time t measured for PRFL in liver. The RF parameters for the three cases are: V(peak) = 90 V, D = 10 ms, and N = 1 Hz; V(peak) = 70 V, D = 20 ms, and N = 1 Hz; and V(peak) = 50 V, D = 20 ms, and N = 2 Hz. The ΔT(avg) at 120 second are: 5.7°C, 6.0°C, and 7.0°C, respectively. Each case would be acceptable in the common clinical paradigm in which V(peak) is set to maintain the tip temperature at 42–44°C for 60–120 seconds, that is, ΔT(avg) = 5–7°C above 37°C. Table 3 shows the calculated and the measured values of ΔT(avg) for PRFL in liver for various parameters and using a constant σ(eff) = 0.29; the agreement is qualitatively reasonable.

Hot Flashes and Hot Spots During PRFL Pulses in Liver

The electric field and temperature distributions during PRFL pulses are highly nonuniform in both the spatial and the time dimensions. Spatially, E reaches local maximum near sharp edges and especially at sharp points. This means that the current density **j**, power deposition P, and tissue temperature T will also have local maxima at these "hot spots." Because all of the RF power in PRFL is delivered in a very short pulse time, tissue temperatures during the pulse time should exhibit a T-spike or "hot flash." The magnitude of the T-spikes depends sensitively on V, D, σ, k, and C_p. To demonstrate the hot spots and hot flashes, finite-element calculations are performed using small space and time scale increments. The results are compared with measurements of T using the very fast-responding micro-TC thermocouple shown in Figure 1.

Figure 10 shows the calculated T-distribution for PRFL at the end of the first t = 20 ms pulse for V(peak) = 45 V, D = 20 ms, N = 2 Hz; and V(peak) = 70 V, D = 20 ms, and N = 1 Hz. The peak temperature at the electrode point is about 44°C and 52°C, respectively, assuming an ambient T of 37°C; that is, the hot flash amplitude is ΔT(peak) = 7°C and 15°C, respectively. The calculation's space grid is about 0.05 mm at the electrode point, and its time grid is 0.2 ms. Figure 10 shows that the hot flash at the point does not spread out more than about 0.3 mm during the pulse. Some spread is into the metal point of the electrode because of the metal's high thermal conductivity. Figure 10 also shows the T-distribution at the end of a later 20 ms pulse and after the pulses have continued for 120 seconds. The average temperature inside the tip, which would be recorded by the SMK-TC macro-TC sensor, has risen about 5–6°C to T = 42–43°C for both cases. At the tip point, the heat spike amplitude ΔT(peak) remains the same as for the first pulse. Peak T at the tip point has risen to about 50°C and 62°C, respectively. Laterally from the electrode's midpoint, T reaches about 45°C near the electrode surface for the 45 V case and is about 44°C at 1 mm away. For the 70 V cases, T = 49°C is about 1.5 mm away.

Table 3 Calculated and measured temperature rises for PRFL

			Calculated		Measured	
Peak Voltage (V)	Pulse Duration (ms)	Pulse Frequency (Hz)	ΔT(avg) at 120 seconds (°C)	ΔT(peak) (°C)	ΔT(avg) at 120 seconds (°C)	ΔT(peak) (°C)
50	20	2	7.8	8.6	7	7
70	20	1	8.9	21.1	6	15
70	20	2	15.9	21.3	—	15
90	10	1	7.7	18.6	6	15.5
90	20	1	11.8	28.3	—	25

PRFL = pulsed radiofrequency lesioning.

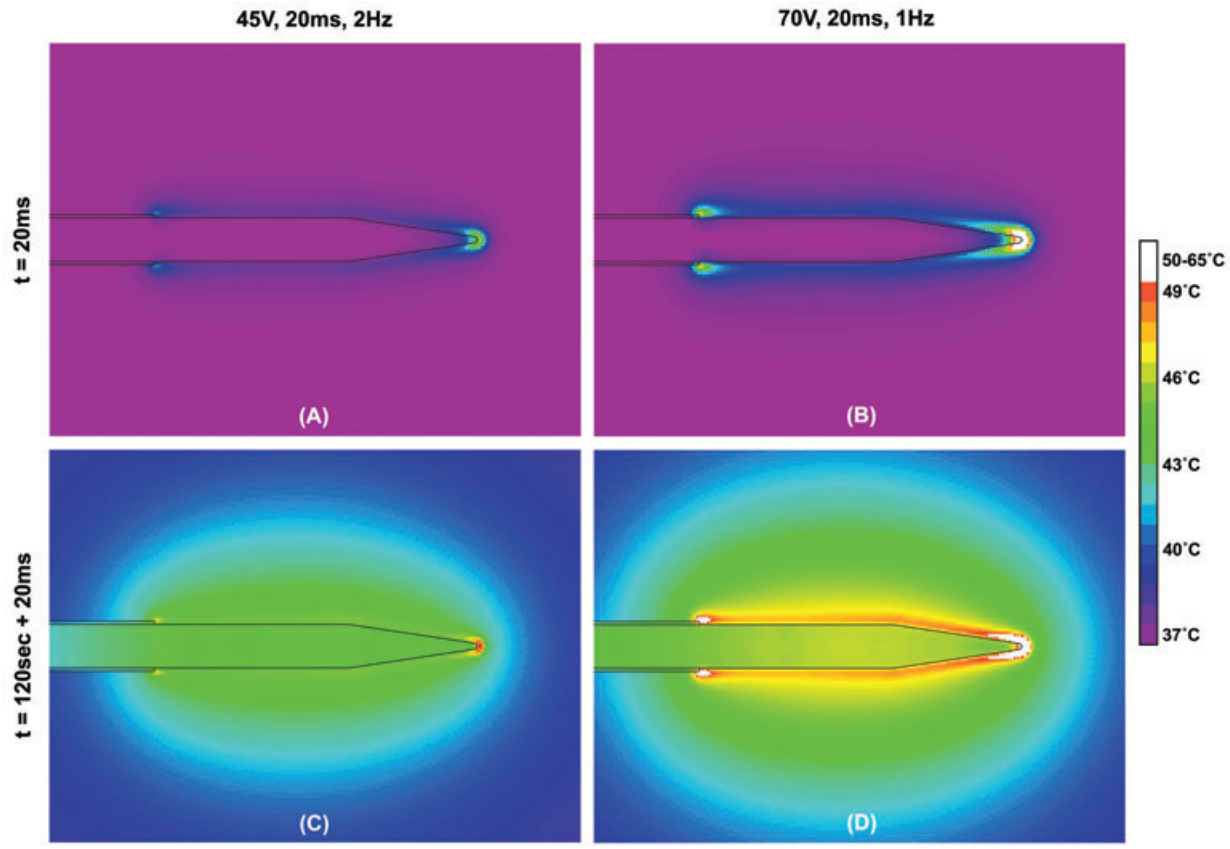

Figure 10 The *T*-distribution at the end of two PRFL pulses for the cases: *V*(peak) = 45 V, *D* = 20 ms, and *N* = 2 Hz; and *V*(peak) = 70 V, D = 20 ms, and *N* = 1 Hz. The first pulse at *t* = 20 ms is shown on top parts A and B. The pulse at *t* = 120 seconds plus 20 ms is shown on the bottom in parts C and D. PRFL = pulsed radiofrequency lesioning.

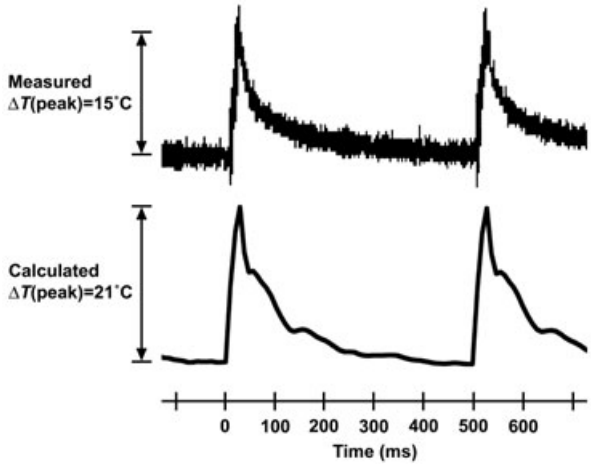

Figure 11 Temperature spikes during PRFL pulses in liver. On the top is shown the measured *T*-spikes for *V*(rms) = 70 V, *D* = 20 ms, *N* = 2 Hz, and on the bottom is the calculated prediction. PRFL = pulsed radiofrequency lesioning.

Figure 11 shows *T* versus time profiles of PRFL heat spikes in liver using *V*(peak) = 70 V, *D* = 20 ms, and *N* = 2 Hz. The upper graph is measured from the micro-TC sensor at the electrode point. *T* rises to a heat spike maximum of ΔT(peak) = 15°C in 20 ms. *T* falls off after the pulse in an exponential decay until the next pulse arrives. In the lower graph in Figure 11, the calculated hot flash has ΔT(peak) = 21°C in qualitative agreement with the data.

Figure 12 shows PRFL heat spikes in liver for pulse widths *D* = 20 ms and 10 ms, and for a progression in *V*(peak) values. Qualitatively, it is expected that ΔT(peak) will be proportional to input power (during the peak) times the pulse duration *D*, for very short pulses. That is, ΔT(peak) is proportional to $V(\text{peak})^2 D/2R$. From Figure 12, ΔT(peak) does increase directly as $V(\text{peak})^2$, and for an equal value of *V*(peak), ΔT(peak) for *D* = 10 ms is about 0.6 that for *D* = 20 ms.

Similar heat flashes for PRFL have been measured in egg-white. Because the resistance *R* for

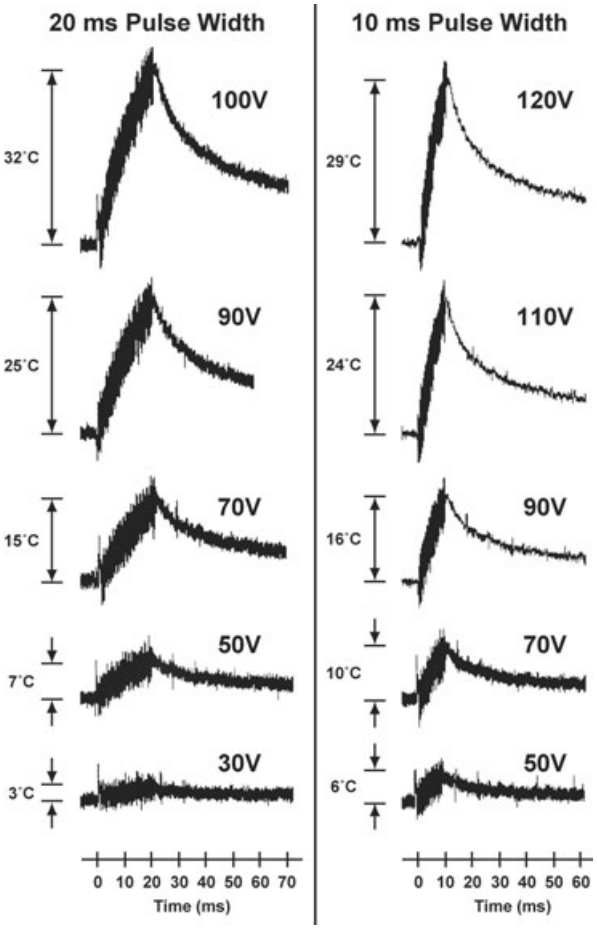

Figure 12 Measured temperature bursts during PRFL pulses in liver at various *V*(peak) settings: on the left for $D = 20$ ms, and on the right for $D = 10$ ms. PRFL = pulsed radiofrequency lesioning.

egg-white is between two and three times lower than for liver, and because ΔT (peak) is proportional to $V(\text{peak})^2 D/2R$, it is expected that ΔT(peak) for egg-white should be between two and three times greater than for liver. This is closely confirmed by the measurements.

Figure 13 is a graph of ΔT(peak) versus the input power $P = 0.5\ V(\text{peak})^2/R$ for $D = 10$ ms and for $D = 20$ ms PRFL pulses, both for liver and egg-white. Two other ordinate axis scales are added to indicate the corresponding *V*(peak) values for liver and egg-white assuming that they have constant resistance values of 287 Ω and 111 Ω, respectively, as measured during the data collection. The ΔT(peak) versus *P* graphs are very close to straight lines as expected. The liver and egg-white graphs for $D = 20$ ms are nearly identical, which confirms consistency of the ΔT(peak) and *R* measurements. The ΔT(peak) value for a given *P* value for $D = 20$ ms is about 1.6 times that for $D = 10$ ms. In the simple model where the PRFL pulse energy is deposited in the tissue instantaneously and there is no thermal conduction, ΔT(peak) for $D = 20$ ms should be two times ΔT(peak) for $D = 10$ ms. The observed differences between the measured and the calculated ratio is consistent with non-negligible heat conduction into the tissue and into the metal tip during the pulse time.

Table 3 shows the calculated and the measured values of ΔT(peak) during PRFL for various parameters. The calculated ΔT(peak) is about 20–30% higher than the measured values. This probably reflects the finite extent of the micro-TC sensor and suggests that the actual *T*-spikes in the tissue are higher than those measured at the electrode tip point by the micro-TC.

Visual confirmation of a PRFL hot spot at the point of the tip is shown in Figure 14. The SMK-C10 with 5 mm tip is viewed by a video microscope during PRFL in egg-white. Egg-white turns

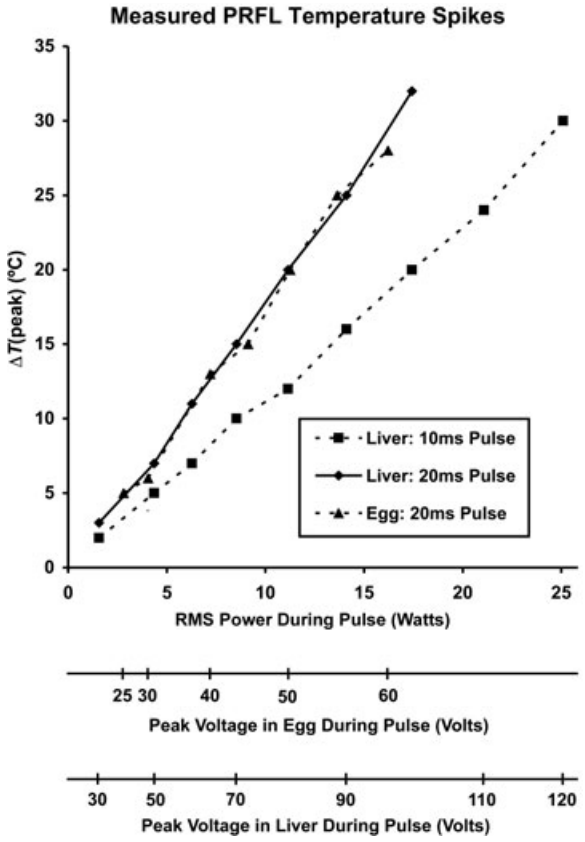

Figure 13 Heat spike amplitudes ΔT(peak) versus average input power during a PRFL pulse for liver and egg-white and for pulse durations of $D = 10$ ms and 20 ms. The two extra ordinate scales show the corresponding *V*(peak) values for liver and egg-white. PRFL = pulsed radiofrequency lesioning.

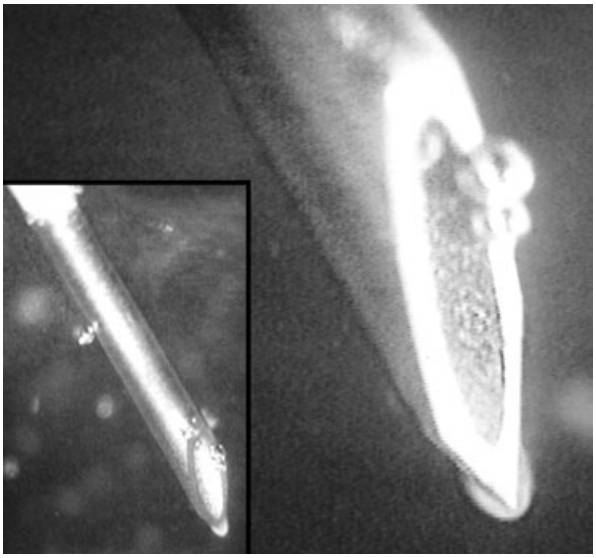

Figure 14 A photograph of the SMK-TC(10)-5 mm electrode in egg-white with evidence of a hot spot at the point tip during PRFL showing as a white volume. PRFL = pulsed radiofrequency lesioning.

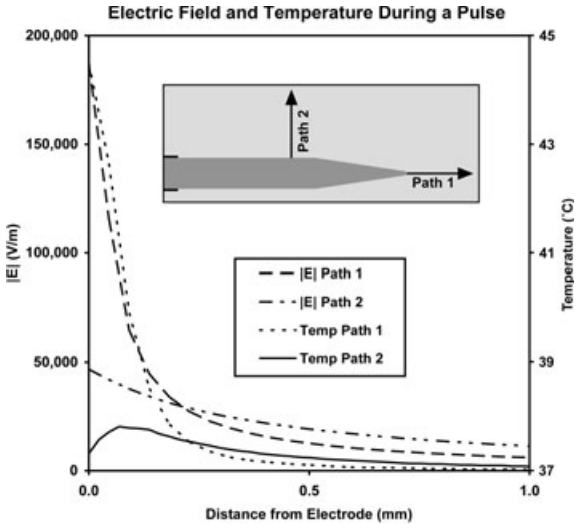

Figure 15 The E-field and T-field magnitudes as a function of distance from the SMK electrode along two different directions for PRFL with V(peak) = 45 V and D = 20 ms. PRFL = pulsed radiofrequency lesioning.

an increasingly dense white color above about 55–60°C, using V(peak) = 70 V, D = 20 ms, and N = 2 Hz, a white volume first begins to form at the tip's point within a few seconds. This shows that the point is indeed the hottest spot on the electrode and the egg-white nearly has exceeded 55–60°C.

Figure 15 shows the calculation predictions of the strengths of the E- and T-fields in PRFL. The PRFL parameters are V(peak) = 45 V and D = 20 ms, values which are commonly used in practice [10]. The E and T curves are plotted as a function of distance from the surface of the electrode tip in two directions: path 1 being from the tip point outward along the axis line of the electrode, and path 2 being from the mid-point of the tip outward laterally. The calculation of T corresponds to the end of the first pulse at t = 20 ms, so that the background level of T has not yet risen. Of course, for a later pulse during the PRFL application at t = 120 seconds, the T-background will have risen by about ΔT(avg) = 5–6°C according to Figure 10, so that the entire T curves will be shifted upward by that amount. The E curve only depends on V(peak) and should remain the same for later pulses.

The distance dependence of both E and T are quite different along paths 1 and 2. Along path 1, E and T drop off rapidly from their peak values of $E \cong$ 200,000 V/m and $T \cong$ 44°C at the point surface to $E \cong$ 10,000 V/m and $T \cong$ 37°C at 1.0 mm away.

Along the lateral path 2, both E and T drop off more slowly with increasing distance, beginning at lower maximum values at the tip surface but sustaining larger values at longer range than path 1. At the surface, $E \cong$ 45,000 V/m and $T \cong$ 37°C, and at a distance of 1.0 mm, $E \cong$ 20,000 V/m and $T \cong$ 37°C.

Figure 16 shows the effects of blood circulation on CRFL lesion size. For an assumed W_b of 10 kg/m^3 s the change in lesion lateral dimension at the 50°C isotherm is about a 15% decrease. This is for a homogeneous tissue model. In reality, the presence of a large artery near the RF electrode can cause significant "cool" spots in the heat lesion distribution.

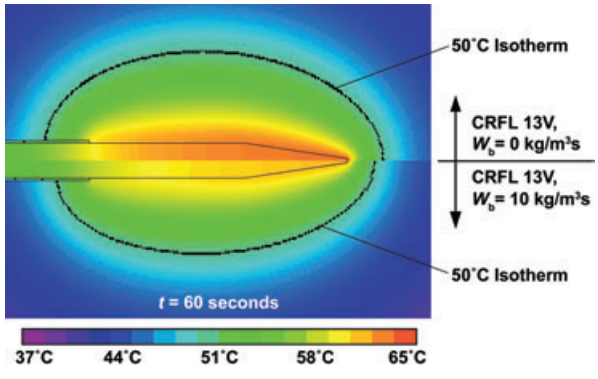

Figure 16 The effect on isotherm volume as calculated with and without blood circulation.

Discussion

Physical Mechanisms in RF Lesioning Processes

An RF signal on an electrode produces two types of basic fields in the tissue: electrical fields and magnetic fields. At 500 KHz, magnetic fields are negligible. It is the electric field **E** that is the origin of all effects we see in RF lesioning, in both CRFL and PRFL. The E-field produces forces on ions and other charged structures. This produces movement of ions in electrolytes, current densities **j**, and stresses on cellular substructures and membranes. Currents **j**, in turn, produce ionic friction and heat, and this then produces the increase in temperature seen in CRFL and PRFL. All of these mechanisms, not just temperature rise, have the potential of producing modifications of neural structures and neuronal behavior when the E-field becomes high enough. All of these mechanisms might be relevant in understanding how RF lesioning produces its effects in pain relief therapy.

Experiments are required to elucidate the importance of each RF mechanism. However, theoretical predictions, when reliable, are essential to guide and to interpret the experiments.

The agreement between the measured ex vivo data on liver and the calculated predictions for the electrode tip temperature and impedance suggest that such calculations can also predict with confidence the E- and T-fields in space and in time-evolution around the electrode in the homogeneous tissue model. Knowing the E- and T-fields in the tissue is an essential step in a quantitative understanding of their effect on neural tissue near the electrode. Because the tissue parameters used for ex vivo liver are very close to those for in vivo neural tissue, the prediction of E- and T-fields described here should be relevant to the clinical RF context. Of course, the tissue environment near clinical targets may not be homogeneous. Large blood vessels, proximity to bone, differences in tissue impedance, and interfaces of fluid and tissue layers of surrounding tissues all can be significant and must be accounted for.

The Thermal and Electrical Effects on Tissue in CRFL Applications

It is generally agreed that raising tissue temperature above the "lethal temperature range" of $T \geq 45$–$50°C$ for 20 seconds or more will destroy cell structures and bio-molecules. Thus, it is useful to know in the CRFL case the expected dimensions of the 45–50°C isotherm volume, and some data on this subject have been collected [3]. An example of the theoretical prediction of lesion size is shown in Figure 6 for the SMK-C10 electrode with 5 mm tip when the tip temperature is 65–70°C. This kind of prediction can be a guide to optimal electrode geometry, electrode position, and tip temperatures to destroy a target.

The type and degree of bio-destruction versus temperature and time for CRFL heat lesions is not fully understood. For example, Dieckmann et al. [11] have studied experimentally the morphology of heat lesions in the living brain of animals. They observed progressive layers of charring, coagulative necrosis, liquification necrosis, demyelinization, etc. as T decreases as a function of distance from the innermost lesion core to an outermost margin which is probably near the 45–50°C margin. Brodkey et al. [12] have shown that "reversible heat lesions" occur between $T = 42.5$ and 44°C in which range temporary cessation of neural activity occurs in brain tissue.

The exact effect on neurons between the 42°C and the 45–50°C margin in a CRFL is unknown. Is the "reversible heat lesion" of Brodkey et al. really a temperature effect, and if so, what is the nature of the neuronal changes and what are the time and temperature dependencies of such effects? Or is the so-called reversible heat lesion effect actually caused by nonthermal E-field effects? It is noted that $E \cong 2{,}500$ V/m at the 50°C isotherm in Figure 6 for CRFL $V(\text{rms}) = 13$ V. This E-field is large in biological terms. The number of neurons exposed to comparable E-fields in the zone between 50–45°C and 42°C is proportional to the volume of the shell between the 50–45°C isotherm and the 42°C isotherm. The shell volume is proportional to the area of the 50°C isotherm surface times the thickness of the shell. That shell volume is significant compared with the "heat lesion volume" itself, so the total effect, including the "reversible heat lesion effect," on the neurons within that volume should also be significant.

Thus, although CRFL heat lesions unquestionably have a dominant component involving heat destruction of cell structures, it is unclear what other E-field effects may be involved. It is premature to describe CRFL as being all-thermal effects and no other E-field effect. Here again the calculated prediction of E and T at the margin of the heat lesion can be insightful.

The Thermal and Electrical Effects on Tissue in PRFL Applications

PRFL and CRFL originate from the same underlying physical laws, but differ in space, time, and

strength of resultant fields. From this study, PRFL can be characterized as having typically much stronger E-fields than CRFL, and also as having temperature spikes above the average thermal background elevation that can extend well into the 45–50°C levels. In a frequently adopted practice of holding the average T background at or somewhat below about 42°C, PRFL also differs from CRFL in that the spatial extent of continuously elevated temperatures is much less than the CRFL.

The effect on neurons of a sustained stream of short heat bursts above 45–50°C is unknown. If the effect in PRFL of such a "thermal dose" is significant, then it is likely to be dependent on the heat spike amplitudes, durations, pulse rates, the total number of heat spikes, and the total exposure time. The mere existence of T-spikes with peak temperatures well above the "lethal temperature level" of 45°C does not necessarily mean that they will destroy cell structures in the same way as CRFL heat lesions. However, the existence of hot flashes indicates that temperature effects must be considered as a potentially significant neurolytic agent in PRFL, and that PRFL cannot be described as a "nonthermal lesion."

The high E-fields encountered in PRFL can have plausibly significant effects on neurons because of the transmembrane potentials U_m that they induce. The order of magnitude of U_m is estimated here using a simplified model shown in Figure 17. The nerve cell is considered a sphere of radius r in a uniform applied RF electric field **E** (the cell could have been considered a cylinder of radius r, and the results would be nearly identical to those described here). The E-lines near the cell can be calculated by Laplace's equation, and their qualitative behaviors are shown. At low E-field frequencies, viz. 1–10 KHz, the membrane is approximately an insulator, and the E-lines curve around the cell. Charges have time to build up on the membrane as shown, and U_m is maximized. Near 1 MHz (MegaHertz = 1,000 KHz), charging times lag the rapid field oscillations, the E-lines partially penetrate the cell, and U_m is reduced. By 100 MHz, the membrane impedance is very small, the E-lines pass straight through the cell, and U_m reduces further. The magnitude of U_m is estimated to be:

$$U_m(\phi) = \frac{1.5Er\cos\phi}{\sqrt{1+(2\pi f\tau)^2}}$$

Where ϕ is the angle shown in Figure 17, τ is a time-constant dependent on membrane dynamics, and f is the RF frequency. The transmembrane potential oscillates between positive and negative extremes with amplitude U_m and frequency f.

Qualitatively, U_m increases with E and with cell radius r, and decreases with increasing frequency f. For V(peak) = 45 V, a typical PRFL value, Figure 15 shows that E = 10–50 KV/m at 1–2 mm laterally and at 1 mm forward of the electrode's tip. Close to the tip's point, E = 100–200 KV/m.

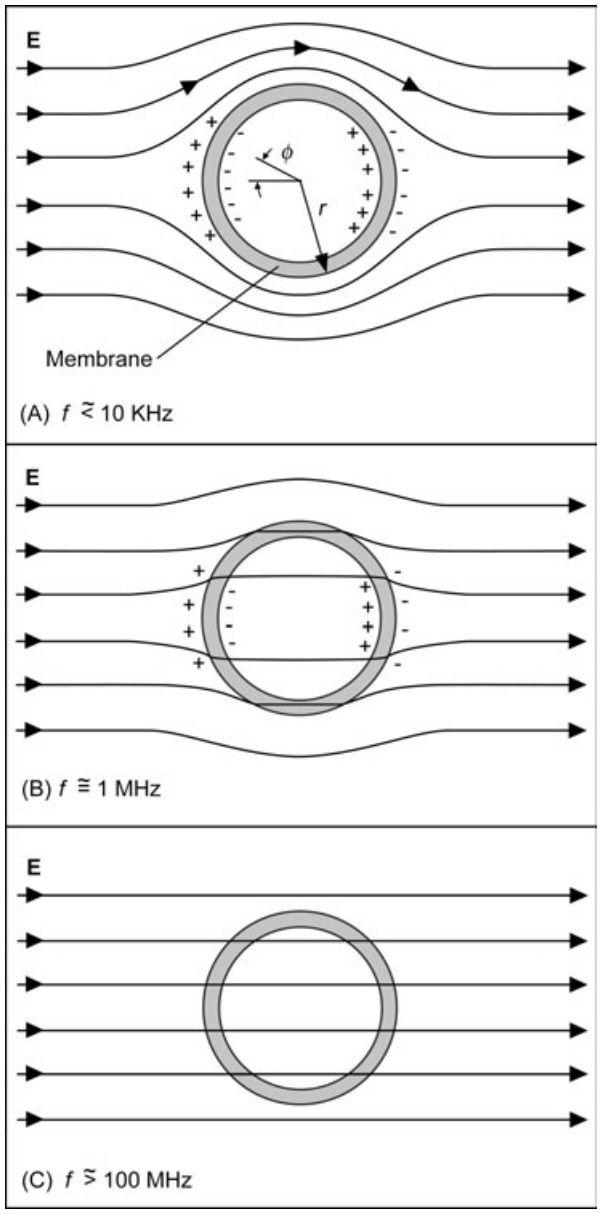

Figure 17 A simplified model of a spherical nerve cell in an applied E-field at different frequencies. The diagram is schematic, and the elements such as membrane thickness to cell diameter are not drawn to scale. (A) $f \cong$ 1–10 KHz; (B) $f \cong$ 1 MHz; (C) $f \geq$ 100 MHz.

Table 4 Estimated maximal transmembrane potential amplitudes U_m(max) during PRFL

	U_m(max) = 1.5 Er		
E (KV/m)	C-Fibers $r \cong 0.5$ μm	Aδ-Fibers $r \cong 2.0$ μm	A-Motor Fibers $r \cong 5.0$ μm
10	0.008	0.03	0.08
50	0.04	0.15	0.4
100	0.08	0.3	1.0
400	0.3	1.2	3.0

PRFL = pulsed radiofrequency lesioning.

In the Results section, it is shown that an acceptable PRFL parameter set that holds T(avg) at 42–43°C includes V(peak) = 90 V, D = 10 ms, and N = 1 Hz. This doubles the E values just cited, reaching 100–400 KV/m at the tip. For the possible range of E = 10–400 KV/m, the U_m-range is equally wide. Assuming for the moment that the denominator in the U_m-equation is one (the low-frequency limit), the maximum U_m values are at the poles of the cell where $\phi = 0°$ and 180° and $\cos\phi = 1$, and are given by $U_m(\max) = 1.5\,Er$. Table 4 shows the range of U_m(max) in PRFL for C, Aδ, and A-motor fibers with nominal radii of r = 0.5, 2.0, and 5.0 μm, respectively. U_m-effects should be greatest at the nodes of Ranvier. Although C-fibers have more unmyelinated exposure, U_m-effects would likely be selectively larger for Aδ-fibers over C-fibers because of the larger radius of the former. U_m-effects can also occur for non-neural cells, which can secondarily affect the neural environment.

Various model-dependent factors can either reduce or increase these U_m values. For instance, the denominator in the U_m-equation produces an attenuation of U_m at higher frequencies. This is important to the estimates of U_m(max) in PRFL because the critical frequency $f_c = 1/(2\pi\tau)$ above which this attenuation becomes significant is probably close to the RF frequency of 500 KHz used in PRFL. We estimate $\tau \cong 1$–2 μs, which implies that U_m(max) would be reduced by about a factor of 3–6 from those in Table 4 at 500 KHz. A recent calculation of electroporation by E-field, which accounts for multicellular and heterogeneity factors, suggests that the attenuation at 500 KHz is not that large and may even be zero in some circumstances [13].

In the following sections, possible effects of high fields and transmembrane potentials on neurons are suggested and may be avenues for future investigation.

Destructive and Disruptive Effects of RF Heat, High *E*, and High *j*

There is physical evidence that both CRFL and PRFL produce destruction and disruption of neurons. For CRFL, the destruction by heat above about 70°C is macroscopically visible as described above. For CRFL from 45°C to 70°C, heat damage is more subtle. Erdine et al. [14] showed that for CRFL on the DRG of rabbits at 67°C, DRG neurons appeared normal under light microscopic analysis. However, under electron microscopic analysis, the 67°C CRFL showed a microscopic destruction and disruption involving structures inside the cell.

Physical evidence has also shown that the PRFL is destructive and disruptive to neurons. Cahana et al. [15] performed PRFL on hippocampal cell cultures using an SMK electrode, T(avg) = 38 and 42°C, D = 20 ms, N = 2 Hz, V(peak) typically at 35–45 V, and t = 120 seconds. At distances of 0.5 mm from the electrode tip point, there was complete destruction of all neurons.

Erdine et al. [14] performed PRFL on the DRG of rabbits, using the SMK electrode with T(avg) = 42–43°C, V(peak) ≅ 45 V (and was adjusted to hold 42–43°C), D = 20 ms, N = 2 Hz, and t = 120 seconds. Neural tissue appeared normal under light microscopic analysis. Under electron microscopic analysis, the DRG cells showed microscopic disruption of cell substructures, less extensive than that for the 67°C CRFL. In both the PRFL case and the 67°C CRFL, there was microscopic destruction of the normal order of the neurons.

There is indirect clinical evidence of injury to tissue from CRFL and PRFL. In the case of CRFL of the medial branch or the DRG, patients often experience a period of irritative symptoms lasting weeks or months. In the case of PRFL, Sluijter [10], W. E. Cohen (private communication), and K. E. Vogel (private communication) describe that for a significant proportion of patients having a PRFL of the DRG, using typically V(peak) ≅ 45 V and T(avg) ≅ 42°C, there is a three-phase period of recovery. In phase one, pain relief is often immediate and lasts for a day or so. In phase two, there are irritative symptoms and a waxing and waning of relief lasting up to 4–6 weeks. In phase three, the irritation subsides, and there is pain relief for an extended time, often years. Both the irritation period of CRFL and the irritation (phase two) period of PRFL may be indications of healing of tissue following RF damage to cells. Discomfort

from healing of injured tissue often follows a similar pattern, beginning within hours after the insult and lasting for weeks as inflammation, scarring, and neural reactions run their course.

The original published clinic work on PRFL [4] stated that it was nondestructive, as there were no obvious sensory deficits following the procedure. Based on the evidence since then, that statement must be re-examined to account for cellular damage at a microscopic level.

The most likely agents of RF neural destruction and injury are heat, high electric fields, and high current fields. They all originate from **E**, but act in different ways. Heat is a rapid thermodynamic spread of energy among all tissue excitations down to the molecular level, characterized by a global parameter T. Thus, it is plausible that the kind of damage to tissue by a CRFL at 55°C, say, and a PRFL heat spike at 55°C is the same.

Tissue disruption by high E-fields would be more specific than by heat. The E-field induces charges on tissue and produces forces on charged molecular structures, causing them to distort and dislocate. E-field gradients produce dielectrophoretic forces on charged objects, causing stress, distortion, and movement. All such effects can happen at sub-cellular and bio-molecular levels without substantially elevating temperature. They all could disrupt cell function. For instance, any change in ion channel conductances across the neuron membrane would change its function. Ion channels and pumps are known to be delicate composites of charge proteins that control the conduction of Na^+, K^+, Ca^{2+}, Cl^-, and other ions vital to cell function. It is conceivable that violent 500 KHz agitation of structures by large PRFL E-fields could disrupt or modify them. Any temporary or permanent changes in the ion channels would alter Nernst concentration gradients and thus could alter resting and threshold potentials of neurons that mediate pain sensation.

Current densities $j \cong 10^3$–10^5 A/m^2 are predicted in the present calculations during PRFL. These are very large compared with biophysical levels such as 10 A/m^2 for normal transmembrane current or 10 A/m^2 for cardiac defibrillation. Aside from measurable heating, the effects of such high currents on cell structures and molecules are not known. The sustained jostling of ions and biomolecules and their resultant collisions with other cell structures may be of great significance. Heterogeneous values of σ and ε near tissue interfaces and in conductive fluid channels between lipid layers can cause channeling and magnification of **E** and **j** lines. This will cause focal amplification of E, j, T, and U_m, perhaps on a microscopic scale, both inside and outside the axon. Resulting tissue damage and heat spikes would then exist on a microscopic scale, smaller even than the scale studied in the present work.

Electroporation

There is evidence that induced transmembrane potentials of $U_m = 0.1$–1 V cause nonlinear effects on cell membranes capable of deforming, creating pores in, and rupturing the membrane [16]. This process, known as electroporation, has been studied for pulsed, high E-field situations. Most of the studies involve single-shot, rapid (≅1 ms) pulses. In PRFL, a stream of hundreds of pulses contains thousands of micro-RF pulses in which U_m oscillates with the magnitudes discussed above. If the frequency-dependent attenuation at $f = 500$ KHz is not too great, the levels of U_m(max) in Table 4 make it plausible that electroporation may occur in PRFL, particularly at the electrode's point and for larger Aδ and A-motor fibers. Electroporation at high E-fields is destructive and can be irreversible. It causes large increases in membrane permeability and resulting molecular imbalances in the cell that could lead to cell stress or death. Electroporation at lower E-field strengths may produce temporary pores, resulting in Na^+ and K^+ conduction and pulsatory membrane depolarization at the PRFL rate of $N \cong 2$ Hz.

PRFL Membrane Rectification, Long-Term Depression of Nociception, and a Connection to Conditioning Stimulation

The action of PRFL transmembrane potentials U_m at lower E may produce additional effects. We give one possible theoretical example here that may relate to reduction of nociception.

The neuroscience literature reports that certain types of "low-frequency conditioning stimulation" of neurons induces long-term depression (LTD) of synaptic transmission [17,18]. Here we suggest a mechanism of presynaptic depolarization by membrane rectification that could relate the two effects. As Figure 18 implies, the knowledge about synaptic plasticity and LTD from conditioning stimulation might then help to understand the long-term antinociception observed from PRFL.

Bear and co-workers [17] discovered that prolonged, low-frequency conditioning stimulation (900 pulses, 0.5–3 Hz [pps], 0.1 ms, and voltages just below threshold for producing population spikes) induces LTD of synaptic effectiveness in

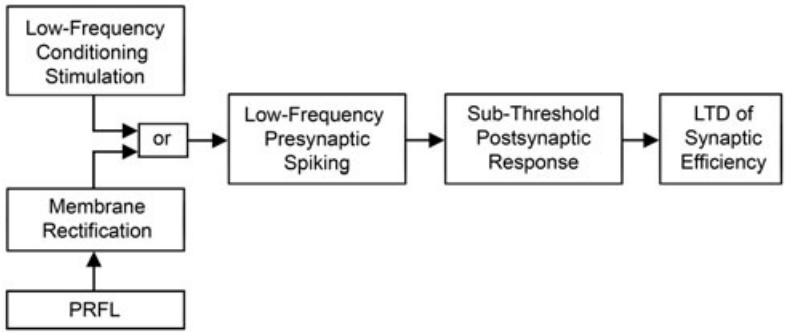

Figure 18 A common mode of action of PRFL and low-frequency conditioning stimulation. PRFL = pulsed radiofrequency lesioning; LTD = long-term depression.

hippocampal neurons. The phenomenon relates to postsynaptic influx of Ca^{+} through N-methyl-D-aspartate (NMDA) receptors. Low-frequency stimulation creates a low level of NMDA activation so that small amounts of Ca^{2+} will enter the postsynaptic neuron, depolarizing it weakly. This activates protein phosphatases, enzymes which alter postsynaptic proteins that mediate LTD.

Sandkühler et al. [18] produced similar LTD of synaptic transmission in primary afferents in the dorsal horn by low-frequency conditioning stimulation of the dorsal roots (900 pulses, 1 Hz [pps], 0.1 ms, and 10–25 V). The effect required stimulation above 8 V, thereby recruiting all Aδ-fibers and not C-fibers and implying Aδ-fiber cooperativity. They proposed that this form of LTD is relevant to long-term afferent antinociception.

The waveforms of PRFL and of conditioning stimulation are dramatically different, so how might they produce the same postsynaptic modification? PRFL at $N = 2$ Hz (pps), $D = 20$ ms, and $f = 500$ KHz has Fourier frequency components bunched at 500 KHz, with no frequencies below that. Conditioning stimulation with 1–2 Hz (pps) and 0.1 ms monophasic pulses has almost all frequency components below 10 KHz, and none near 500 KHz. Two pieces of evidence suggest an answer: 1) Alberts et al. [19] in 1972 showed that bursts of sinusoidal voltages applied to the brain produce stimulative responses up to 150 KHz. The threshold voltage increases dramatically but smoothly with frequency. 2) PRFL does produce a sensory response at higher voltages. The present authors questioned experienced users of PRFL on the DRG: Drs. W. Cohen (private communication), M. Sluijter (private communication), and K. Vogel (private communication). They stated that PRFL frequently induces tingling, pressure, and throbbing parathesia at V(peak) ≅ 25–45 V. This is for the electrode near, but not inside, the DRG, for which the standard stimulation threshold at 50 Hz (pps) is 0.2–0.5 V.

Figure 19 depicts a possible mechanism for current rectification through a schematic membrane and Na^{+} ion channel. The RF transmembrane potential U_m drives Na^{+} ions into the cell on each 1 μs positive RF half-cycle. On each 1 μs negative RF half-cycle, Na^{+} ions are driven out of the cell, but at a lesser amount because of the greater Na^{+} concentration outside of the cell than inside. The net Na^{+} flux in a full 2 μs RF cycle is thus inward, tending toward depolarization. This is Na^{+} membrane rectification. Potassium K^{+} channels (not shown in Figure 19) will rectify K^{+} current outward from the cell in the same U_m cycle because of the higher concentration of K^{+} inside the cell than outside, tending to hyperpolarize the cell. However, the ion channels are voltage-sensitive, and the difference in Na^{+} versus K^{+} conductivity changes for deviations of U_m around the resting potential favors Na^{+} over K^{+} [20]. Thus, the net rectification is inward. For smaller U_m, the average cell potential V_m will be steadily depolarized with time during the PRFL pulse period D and may approach the level of the action threshold. For larger U_m, depolarization could pass the action potential threshold during the PRFL pulse, and the neuron will fire. Further, it could be speculated that for sufficiently large U_m, the first positive RF half-cycle could depolarize the cell over the action threshold immediately, triggering an action potential. In any case, for a PRFL pulse rate of, say, $N = 2$ Hz (pps), the rectification depolarization simulates 2 Hz stimulation. This would explain the observed stimulation responses of PRFL (W. E. Cohen, K. E. Vogel, and M. Sluijter, private communications). The dynamics of ion-channel rectification could explain the frequency-dependence of stimulation threshold for RF signals. A time constant of about 1 ms for ion flow

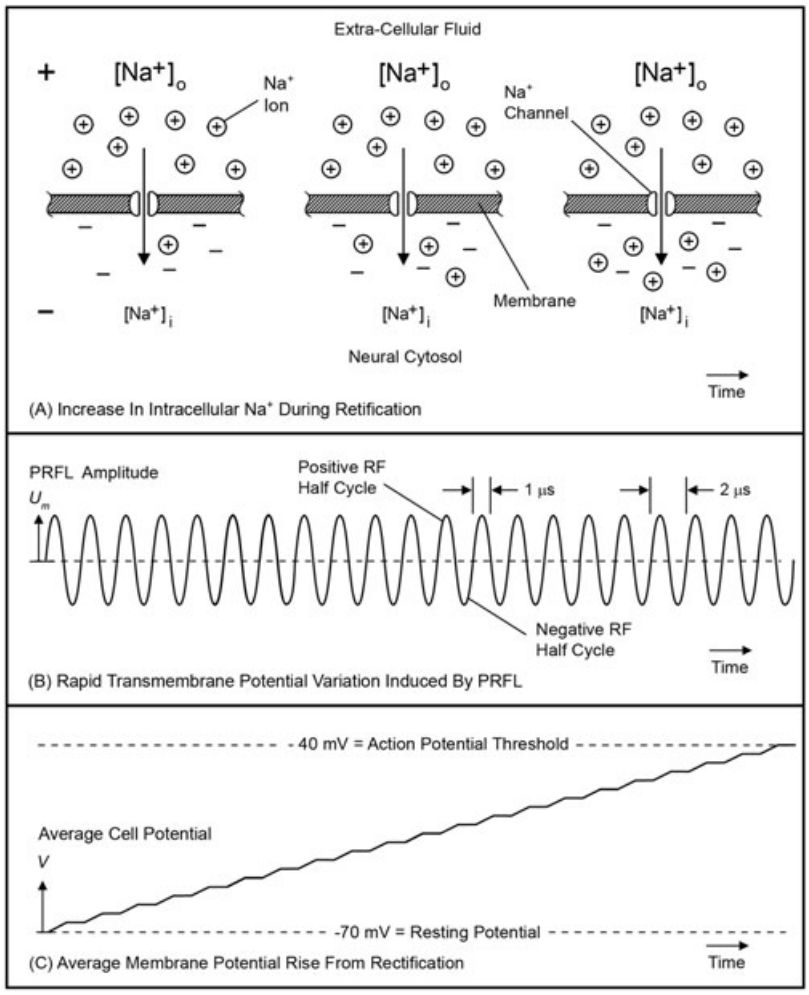

Figure 19 Membrane rectification of current in a neuron from an oscillating transmembrane potential U_m induced by an RF electric field **E**. (A) The concentration of Na^+ ions outside the neuron $[Na^+]_o$ is greater than that inside the cell $[Na^+]_i$. This causes net inflow of Na^+ with time in an oscillating field **E**. (B) The oscillating transmembrane potential U_m during a single PRFL pulse. A full U_m oscillation is 2 μs for an RF frequency $f = 500$ KHz. (C) Net rectification of Na^+ and K^+ currents causes an average depolarization of the neuron's voltage V, as a function of time during the PRFL pulse, leading to an action potential. RF = radiofrequency; PRFL = pulsed RF lesioning.

during rectification (analogous to τ above) is consistent with the data of Alberts et al. [19].

The conditioning stimulation with 0.1 ms monophasic cathodal pulses also induces transmembrane potentials favoring Na^+ influx and depolarization. The similarity to PRFL is that both produce depolarizing pulses at 1–2 Hz (pps). Thus, it is plausible that they should both produce the same postsynaptic modifications, including LTD. If so, following the guideline of conditioning stimulation experience, an effective PRFL protocol would be 900 pulses at $N = 1$–2 Hz (totaling 7–15 minutes) with V(peak) at or just below the threshold for stimulation response [17,18]. This might then achieve LTD of synaptic efficiency and antinociception. These parameters are not far from the ones presently used in PRFL. A test of this proposal can be done by laboratory experiments similar to those of Sandkühler et al. [18], but using PRFL signals instead of conventional stimulation waveforms.

Some evidence of changes in gene expression in the dorsal horn by C-fos formation has been reported both for short-term [21] and long-term [22] periods following PRFL exposure to the DRG in rats. This is suggestive of a possible connection to the present proposal, but the origin of the C-fos formation remains to be clarified.

Optimization of RF Lesioning Parameters

Increased experience with PRFL and better understanding of the underlying E-field and T-field effects on neurons should lead to guidelines for optimal parameters for a desired clinical objective. Such guidelines currently exist for CRFL and include recommendations for the electrode geometry, the average electrode tip temperature, and the lesion time to achieve a desired heat lesion volume for a given procedure [1–3]. However, as this study shows, the properties of the E-field and T-field in PRFL are significantly different than those in CRFL. For instance, although the average

tip temperature is a primary indicator of CRFL efficacy, this is not the case for PRFL. Rather, the RF voltage V is a much better indicator of the E-field and T-field magnitudes in PRFL.

In PRFL, the E-field effects are fractionated over a stream of hundreds of RF pulses extending over an exposure time of several minutes, accumulating millions of RF frequency oscillations, that is, micro E-pulses, in that same time. It is plausible that the end-point effects on neurons will be an "E-dose" function at the neuron's (or cooperative groups of neurons') position. The E-dose is likely to be a graded function of exposure time, with cell changes requiring a statistical number of E-field pulses at a given strength.

The E-dose function should depend on several factors, one being a geometric factor G that accounts for electrode geometry, the distance of the neuron(s) from the electrode, and tissue features. G should also account for tissue inhomogeneities, low-impedance pathways, and the injection of saline into the tissue through the electrode, as these can strongly change the pattern of **E**, **j**, and **T** distributions. The amplitude E is proportional to the voltage V(peak) (or simply V), so V is a fundamental E-dose parameter in PRFL (in an analogous way that tip temperature is the basic scale parameter in CRFL heat effects). E-dose should also depend on a voltage-factor $F(V, f)$ which is a function of V and frequency f. F is likely to have a nonlinear dependence on V. For dissipative processes like heat spikes or for dielectrophoresis forces, F is proportional to E^2, and thus V^2. For transmembrane potential U_m effects, such as electroporation and membrane rectification, F depends on more complex functions of V and f. For dissipative processes, the E-dose may depend on the total time of E-field exposure DNt, which is a product of the pulse duration D, the pulse rate N, and the elapsed time t. In that case, a simplified equation for E-dose at a tissue position **r** from the electrode might be:

$$\text{E-dose}(\mathbf{r}) = GFDNt$$

However, for transmembrane potential effects such as weak electroporation and rectification, the dependence on D and N may be very different, involving limits on these parameters to produce LTD as in the case of conditioning stimulation.

This kind of model of the E-field effect provides a possible framework for optimizing PRFL parameters. For example, knowing the E-dose for one geometry G and voltage factor F could be a guide for selecting an optimal voltage F_1 for another geometry G_1. Knowledge of G for a specific target volume and tissue environment could lead directly to the optimal F to achieve an adequate E-dose to a neural structure. In another circumstance, one may wish to limit F to avoid excessive tissue destruction from T-spikes or electroporation. In this case, one could reduce F (and thus V) below some limiting value and increase DNt accordingly to achieve a desired E-dose. Obviously, DNt can be increased in a number of ways, for example, by increasing the total elapsed time t or increasing the total number of pulses Nt.

Clearly, the interplay of E-dose factors to achieve a desired clinical effect for a given target site warrants further investigation. For example, in the DRG with the electrode near, but outside the DRG, PRFL at $T(\text{avg}) = 42°\text{C}$, $V(\text{peak}) \cong 45°\text{C}$, $N = 2$ Hz, and $t = 2$ minutes seems effective for pain relief but often leads to a period of postoperative discomfort (phase two), probably due to destructive effects of heat spikes or high fields. Perhaps reducing F, by reducing V, and increasing t to maintain the same E-dose would help. Reducing V would reduce $\Delta T(avg)$, reduce heat spikes, and reduce microscopic tissue damage.

Magnetic Field Effects

Magnetic effects induced by E-field-generated currents at 500 KHz are biologically negligible. An estimate of the maximum magnetic field B_{max} which would circulate around the RF electrode is calculated by Ampere's law and is:

$$B_{max} = \frac{\mu_0 I}{2\pi r}$$

Where $\mu_0 = 4\pi \times 10^{-7}$ Tm/A is the permeability of free space, I is the maximum RF current in the electrode, and r is the radial distance from the electrode axis. For example, in the extreme case where the peak RF voltage is 100 V and the electrode impedance is 100 Ω, $I = 1$ Ampere, and at a distance of $r = 1$ mm:

$$B_{max} \cong 2 \text{ Gauss}$$

This is comparable to the earth's magnetic field and is 1,000 times weaker than B-fields in an MRI scanner.

Conclusions

Finite-element calculations closely reproduce the thermal and electrical features of CRFL and PRFL as measured ex vivo. This suggests that they are useful guides to understanding electric, cur-

rent, and thermal fields on macroscopic and microscopic scales.

Both CRFL and PRFL produce tissue temperatures, for commonly accepted parameters, which rise into the so-called lethal temperature range of $T \geq 45$–50°C. CRFL typically produces *T*-distributions more broad in space and time; viz., with ellipsoidal isotherms and time changes on the order of seconds. PRFL *T*-distributions are more localized in space and time; viz., with hot spots at points and edges and heat spike bursts on the order of milliseconds. The differences are ones of macro versus micro lesion scales. However, in view of these findings, it is inaccurate to describe PRFL as a "nonthermal lesion."

The calculated predictions of E, j, and T-fields for PRFL indicate that they are capable of significant, and perhaps destructive, effects on neurons. Possible effects of interest include heat spikes exceeding 45–50°C, high transmembrane potentials, and electroporation. Data exist that show PRFL can be destructive and disruptive to neurons. Thus, it is premature to describe PRFL as "nondestructive," as destructive effects are expected to be at a microscopic, even subcellular, level that to date have not been well examined.

Acknowledgments

The authors thank Ray Fredricks for his help in collecting the experimental data in this study. They also thank Niels Cosman for his help in the preparation of figures.

References

1 Cosman BJ, Cosman ER. Guide to Radio Frequency Lesion Generation in Neurosurgery. Burlington, MA: Radionics; 1974.
2 Cosman ER, Cosman BJ. Methods of making nervous system lesions. In: Wilkens RH, Rengachary SS, eds. Neurosurgery. New York: McGraw-Hill; 1984:2490–9.
3 Cosman ER, Nashold BS, Ovelman-Levitt J. Theoretical aspects of radiofrequency lesions in the dorsal root entry zone. Neurosurgery 1984;15:945–50.
4 Sluijter ME, Cosman ER, Rittman WJ, Van Kleef M. The effects of pulsed radiofrequency fields applied to the dorsal root ganglion—A preliminary report. Pain Clin 1998;11(2):109–18.
5 Johnson C. Numerical methods for bioelectric field problems. In: Bronzino JD, ed. Biomedical Engineering. Boca Raton, FL: CRC Press; 1995:162–80.
6 Humphries S. Field Solutions on Computers. 1st edition. Boca Raton, FL: CRC Press; 1997.
7 Ludt H, Herrmann HD. In vitro measurement of tissue impedance over a wide frequency range. Bio Physik 1973;10(4):337–45.
8 Foster KR, Schwan HP. Dielectric properties of tissues. In: Polk C, Postow E, eds. Biological Effects of Electromagnetic Fields, 2nd edition. Boca Raton, FL: CRC Press; 1996.
9 Cosman ER, Rittman WJ, Nashold BS, Makachinas TT. Radio frequency lesion generation and its effects on tissue impedance. Appl Neurophysiol 1998;51:230–42.
10 Sluijter M. Radiofrequency. Meggen, Switzerland: Flivo Press SA; 2001.
11 Dieckmann G, Gabriel E, Hassler R. Size, form, and structural peculiarities of experimental brain lesions obtained by thermocontrolled radiofrequency. Confin Neural 1965;26:134–42.
12 Brodkey JS, Miyazaki Y, Ervin FR, Mark VH. Reversible heat lesions with radiofrequency current: A method of stereotactic localization. J Neurosurg 1964;21:49–53.
13 Gowrishankar TR, Weaver JC. An approach to electrical modeling of single and multiple cells. Proc Nat Acad Sci USA 2003;100(6):3203–8.
14 Erdine S, Yucel A, Cunen A, et al. Effects of pulsed versus conventional radiofrequency current on rabbit dorsal root ganglion morphology. Eur J Pain 2005;9(3):251–6.
15 Cahana A, Vutskits L, Muller D. Acute differential modulation of synaptic transmission and cell survival during exposure to pulsed and continuous radiofrequency energy. J Pain 2003;4(4): 197–202.
16 Weaver JC. Electroporation: A general phenomenon for manipulating cells and tissue. J Cell Biochem 1993;51:426–35.
17 Bear MF. Bidirectional synaptic plasticity: From theory to reality. Phil Trans R Soc Lond B 2003; 358:649–55.
18 Sandkühler J, Chen JG, Cheng G, Randic M. Low-frequency stimulation of afferent Aδ-fibers induces long-term depression at primary afferent synapses with substantia gelatinosa neurons in the rat. J Neurosci 1997;17:6483–91.
19 Alberts WW, Wright EW, Feinstein B, Gleason CA. Sensory responses elicited by subcortical high frequency electrical stimulation in man. J Neurosurg 1972;36:80–2.
20 Hodgkin A, Huxley AF. The components of membrane conductance in the giant axon of Loligo. J Physiol Lond 1952;116:473–96.
21 Higachi Y, Nashold BS, Sluijter M, Cosman ER, Perlstein RD. Exposure of the dorsal root ganglion in rats to pulsed radiofrequency current activates dorsal horn lamina 1 and 2 neurons. Neurosurgery 2002;50(4):850–6.
22 Van Zundert J, deLouw AJA, Joosten EAJ, et al. Pulsed and continuous radiofrequency current adjacent to the cervical dorsal root ganglion of the rat induces late cellular activity in the dorsal horn. Anesthesiology 2005;102:125–31.